Experimental Validation of UWB-Based Fault-Tolerant Control for Quadcopters Subject to Actuator Failures

Minh Long Lam [1], Cong-Thanh Pham[*1] , Huynh Quang-Duc Lam[1]

[1] Faculty of Electricity and Electronics, Vietnam Aviation Academy

*Corresponding Author/Email: thanhpc@vaa.edu.vn

Manuscript received: April 04, 2026 / Revised: May 05, 2026 / Accepted: May 26, 2026

ABSTRACT

This paper presents a fault-tolerant control algorithm for a four-rotor unmanned aerial vehicle (quadcopter) using an Ultra-Wideband (UWB) positioning system. The proposed control system allows the vehicle to maintain flight stability and position control capability even in the case of a partial actuator failure (motor efficiency degradation). The approach is based on a combination of reconfigurable control, adaptive control, and an observer-based state/los+s monitor. The validity of the method is demonstrated through Lyapunov stability mathematical analysis and verified by real-world flight experiments in an indoor environment using UWB. Experimental results show that the system maintains attitude stability, position hold, and altitude with acceptable errors when a fault occurs, thereby confirming the feasibility and effectiveness of the controller.

KEYWORDS: Quadcopter, UWB Localization, Reconfigurable Control, Adaptive Control, Observer.

1. Introduction

The safety and reliability of quadcopters remain significant challenges, particularly in GPS-denied environments or applications requiring high safety standards. In practice, incidents such as motor thrust degradation or positioning sensor failures can lead to instability and severe accidents.

Ultra-Wideband (UWB) positioning systems have emerged as an effective solution for indoor localization with centimeter-level accuracy. Nevertheless, UWB itself is susceptible to noise, signal occlusion, and measurement errors. Consequently, integrating UWB with fault-tolerant control (FTC) strategies is essential to ensure the safe and continuous flight capability of the quadcopter [1,2,3,7].

In this paper, we experimentally evaluate a UWB-based fault-tolerant control system, in which motor faults are detected and estimated via an observer. Subsequently, the controller is adaptively reconfigured to compensate for the effects of these faults [4,5,6].

2. Quadcopter Mathematical Model with Actuator Faults

The translational and rotational dynamics of the quadcopter in the inertial reference frame can be described as follows:

$$m\dot{v} = R(\eta)\, f_T + mg + d_t J\dot{\omega} = \tau - \omega \times J\omega + d_r \quad (1)$$

where m is the total mass, R(η) denotes the rotation matrix from the body-fixed frame to the inertial frame, τ is the control torque vector, and dt, dr are the unknown disturbances.

Motor faults are modeled as effectiveness degradation: $f_i = \alpha_i f_i^{cmd}$, $0 < \alpha_i < 1$. With αi is the effectiveness coefficient of the i-th motor. The case of a motor fault with performance degradation corresponds to $\alpha_i > 0$.

2.1. Fault-Tolerant Controller and Observer Design Adaptive Observer

The state vector of the estimator is defined as:

$$x = \begin{bmatrix} p & v & \phi & \theta & \psi \end{bmatrix}^T;$$
$$p = \begin{bmatrix} p_x & p_y & p_z \end{bmatrix}^T; \quad (2)$$
$$v = \begin{bmatrix} v_x & v_y & v_z \end{bmatrix}^T$$

Where p denote the position coordinates, v represent the translational velocities, and $\phi,\ \theta,\ \psi$. correspond to the roll, pitch, and yaw angles, respectively.

An Extended State Observer (ESO) is designed to simultaneously estimate the system states, disturbances, and motor faults:

$$\dot{\hat{x}} = f(\hat{x}, u) + L(y - \hat{y}) \quad (3)$$

According to equation (3), ESO estimates: state, total noise and motor efficiency. Where L is the observer gain matrix, chosen such that the observation error converges asymptotically near zero.

Reconfigurable Control Law is formulated as follows:

$$u = \hat{B}^{-1}\left(-Kx - \hat{d}\right) \quad (4)$$

Where $\hat{B}$ is the control allocation matrix, which is adaptively updated based on the motor fault estimation.

Stability Analysis

We propose the following Lyapunov candidate function:

$$V(x,\tilde{\alpha}) = x^T P x + \tilde{\alpha}^T \Gamma^{-1} \tilde{\alpha} \quad (5)$$

Where :

$x \in R^n$: closed-loop system state vector

$\tilde{\alpha} = \alpha - \hat{\alpha}$: fault estimation error.

$P = P^T > 0$: solution to the Lyapunov equation

$\Gamma = \Gamma^T > 0$: adaptive gain matrix

Furthermore, it can be proven that $\dot{V} \le 0$, ensuring the asymptotic stability of the closed-loop system even in the presence of faults.

Since P > 0 and $\Gamma^{-1} > 0$ $\Rightarrow$ The Lyapunov function is positive definite, $V(x,\tilde{\alpha}) \neq (0,0)$ and $V(0,0) = 0$ $\Rightarrow$ V which implies that V is a valid Lyapunov function.

When modeling a fault-affected system, assume that the closed-loop system is subjected to parametric faults:

$$\dot{x} = Ax + B\left(u + \alpha^T \varphi(x)\right) \quad (6)$$

With :

α: Fault or uncertainty vector (actuator fault, efficiency loss, bias…)

φ(x): known regression function.

Fault-compensation control law :

$u = u_0 - \hat{\alpha}^T \varphi(x) \Rightarrow$ The error

$\dot{x} = Ax + B\tilde{\alpha}^T \varphi(x)$

The time derivative of the Lyapunov function:

$$\dot{V} = \dot{x}^T P x + x^T P \dot{x} + 2\tilde{\alpha}^T \Gamma^{-1} \dot{\tilde{\alpha}} \quad (7)$$

Substituting $\dot{x}$ into:

$$\dot{V} = x^T \left(A^T P + PA\right) x + ... \quad ...+2x^T PB\varphi^T \tilde{\alpha} + 2\tilde{\alpha}^T \Gamma^{-1} \dot{\tilde{\alpha}} \quad (8)$$

From the Lyapunov equation, choose P such that:

$A^T P + PA = -Q$, $Q = Q^T > 0$

$$\Rightarrow \dot{V} = -x^T Q x + 2\tilde{\alpha}^T \left(\phi(x) B^T P x + \Gamma^{-1} \dot{\tilde{\alpha}}\right) \quad (9)$$

Fault Estimation Law

Select the parameter update law as follows

$$\dot{\hat{\alpha}} = -\Gamma \phi(x) B^T P x \quad (10)$$

$$\Rightarrow \dot{\tilde{\alpha}} = \Gamma \phi(x) B^T P x \quad (11)$$

From equation (10), we also use the error update law with limits in the actual firmware as follows: $0 < \alpha_i < 1$. A fault admissible set is $\alpha_i > 0.4$ necessary to ensure stability. Here, we set $\alpha_i = 0.5$ to ensure system safety (Tab 1).

Table 1: Description of engine performance limits according to error update law.

Motor performance	Status
1.0	normal motor
0.8	Reduced thrust slightly
0.5	weak motor
0.0	completely lost

Substituting into $\dot{V}$:

$$\dot{V} = -x^T Q x < 0 \quad (12)$$

$\dot{V} < 0 \Rightarrow$ Stability in the sense of Lyapunov

$x(t), \tilde{\alpha}(t)$ Bounded

According to LaSalle's Invariance Principle

However, it is important to state that the maximum invariant set of $\dot{V} = 0 \Rightarrow x = 0$

$$\Rightarrow \lim_{t \to \infty} x(t) = 0 \quad (13)$$

Formula (13) only shows the trajectory converging to the invariant set. But it does not guarantee that the invariant set is the desired stable flight state; the system will become severely unstable.

A model that is most complete and consistent is

$$x = \left[\, xyzv_x v_y v_z \phi\theta\psi\, pqr \,\right]^T \quad (14)$$

Table 2: Meaning of variables based on the complete and consistent model of (14)

Variable	Meaning
x,y,z	location
v_x, v_y, v_z	speed
ϕ	roll
θ	pitch
ψ	yaw
pqr	angular rates

Actuator failure model in the case of engine performance degradation:

$0 < \alpha_i < 1$

Thus, Total Thrust is written as follows:

$T = \sum_{i=1}^{4} \alpha_i k_f \omega_i^2$

The control moments include:

Roll torque:

$\tau_\phi = l k_f \left(-\alpha_1 \omega_1^2 + \alpha_2 \omega_2^2 + \alpha_3 \omega_3^2 - \alpha_4 \omega_4^2\right)$

Pitch torque:

$\tau_\theta = l k_f \left(\alpha_1 \omega_1^2 + \alpha_2 \omega_2^2 - \alpha_3 \omega_3^2 - \alpha_4 \omega_4^2\right)$

Yaw torque:

$\tau_\psi = k_T \left(-\alpha_1 \omega_1^2 + \alpha_2 \omega_2^2 - \alpha_3 \omega_3^2 + \alpha_4 \omega_4^2\right)$

With generalized vector input, the FTC essentially controls:

$U = \left[\, T \tau_\phi \tau_\theta \tau_\psi \,\right]^T$

With the allocation matrix, we have the following relationship:

$U = B_f u$

Where

$$B_f = \begin{bmatrix} \alpha_1 k_f & \alpha_2 k_f & \alpha_3 k_f & \alpha_4 k_f \\ -l k_f \alpha_1 & l k_f \alpha_2 & l k_f \alpha_3 & -l k_f \alpha_4 \\ l k_f \alpha_1 & l k_f \alpha_2 & -l k_f \alpha_3 & -l k_f \alpha_4 \\ -k_T \alpha_1 & k_T \alpha_2 & -k_T \alpha_3 & k_T \alpha_4 \end{bmatrix}$$

This is the fault-dependent control allocation matrix of formula (4).

Dynamics, according to Newton:

$$m\ddot{p} = R(\phi,\theta,\psi)\begin{bmatrix}0\\0\\T\end{bmatrix} - \begin{bmatrix}0\\0\\mg\end{bmatrix} + d_t \quad (15)$$

Where
R: rotation matrix
d_t: disturbance
Rotation matrix: $R = R_z(\psi)R_y(\theta)R_x(\phi)$
Rotational dynamics, Euler rigid body dynamics:

$$J\dot{\Omega} + \Omega \times J\Omega = \tau + d_r \quad (16)$$

where
$\Omega = [pqr]^T$
and
$\tau = [\tau_\phi \tau_\theta \tau_\psi]^T$
Euler angle kinematics: $\dot{\eta} = W(\phi,\theta)\Omega$ (17)
where $\eta = [\phi\theta\psi]^T$
and $W(\phi,\theta) = \begin{bmatrix}1 & \sin\phi\tan\theta & \cos\phi\tan\theta\\ 0 & \cos\phi & -\sin\phi\\ 0 & \sin\phi/\cos\theta & \cos\phi/\cos\theta\end{bmatrix}$
Commonly used FTC/adaptive observers:

$$\dot{x} = f(x) + g(x)B_f u + d \quad (18)$$

where
$f(x)$: nonlinear rigid-body dynamics
$g(x)$: input distribution
B_f : fault allocation matrix
d: disturbances
If linearize around a state of suspended equilibrium, we have:

$$\dot{x} = Ax + B_f u + d \quad (19)$$

where
A: linearized system matrix
B_f : fault-dependent input matrix
We integrate faults using multiplicative actuator effectiveness, which means:
$u_{actual} = diag(\alpha_1, \alpha_2, \alpha_3, \alpha_4)u_{command}$
Therefore, fault does not add up like disturbance does, but rather fault changes control authority in the FTC.
Our quadcopter model is Nonlinear fault-dependent:

$$\dot{x} = f(x) + g(x)B_f(\alpha)u + d \quad (20)$$

where
status $x = [pv\eta\Omega]^T$
Actuator errors are integrated using $\alpha_i \in (0,1)$
Faults directly alter the system's thrust, torque, control allocation matrix, and controllability margin.
Therefore, the closed-loop system remains locally asymptotically stable under partial actuator effectiveness loss, provided that the control allocation matrix preserves sufficient rank and actuator authority. The proposed adaptive fault-compensation law ensures robustness and stability without requiring precise fault information [6, 8]. Quadcopter configuration showing the distribution of four motors with ESP32 - Wroom 32 as the Flight Controller (UWB Tag not yet attached).

2.2. Experimental Setup

To improve the reliability of indoor localization under UWB measurement noise and temporary signal degradation, the proposed system employs an IMU–UWB sensor fusion framework based on an Extended Kalman Filter (EKF). The EKF combines high-frequency inertial measurements from the ICM20602 IMU with absolute position measurements obtained from the DWM1000 UWB localization system.
The prediction step of the EKF utilizes the IMU measurements:

$$x_{k+1} = f(x_k, u_k) + w \quad (21)$$

where (u_k) contains the accelerometer and gyroscope data, and (w_k) represents process noise.
The UWB localization measurements are incorporated during the correction stage according to:

$$z_k = Hx_k + v_k \quad (22)$$

Where (z_k) is the UWB position measurement vector and (v_k) denotes measurement noise.
The IMU provides high-rate attitude and acceleration information, while the UWB system supplies drift-free absolute position updates. Consequently, the fusion framework improves robustness against temporary UWB signal occlusion and reduces the drift associated with standalone inertial navigation.
The overall control architecture is illustrated in Fig. 1, where the EKF-based sensor fusion block provides the estimated states to the fault-tolerant controller and adaptive observer. The observer estimates actuator effectiveness degradation, and the control allocation matrix is reconfigured online to maintain stable flight performance under motor fault conditions.

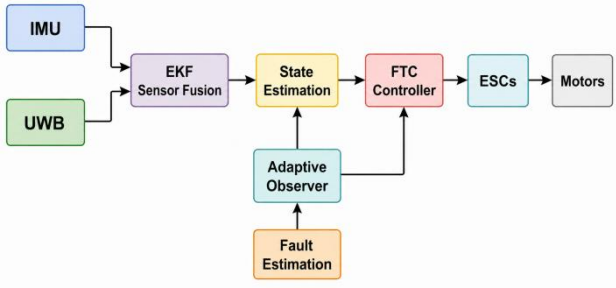

Figure 1: Overall architecture of the proposed IMU–UWB fusion-based fault-tolerant control system.

The proposed architecture integrates IMU and UWB measurements through an Extended Kalman Filter (EKF)-based sensor fusion framework to obtain accurate state estimation. The estimated states are subsequently utilized by the Fault-Tolerant Control (FTC) system to generate robust control commands for the Electronic Speed Controllers (ESCs) and motors. In parallel, an adaptive observer is employed to estimate actuator faults and uncertainties in real time. The estimated fault information is then fed back to the FTC controller to enhance system reliability and maintain stable

operation under fault conditions. The key point in this architecture is that the FTC doesn't shut down faulty motors or switch to emergency mode; the drone still uses all four motors, but the response weighting is based on motor performance.

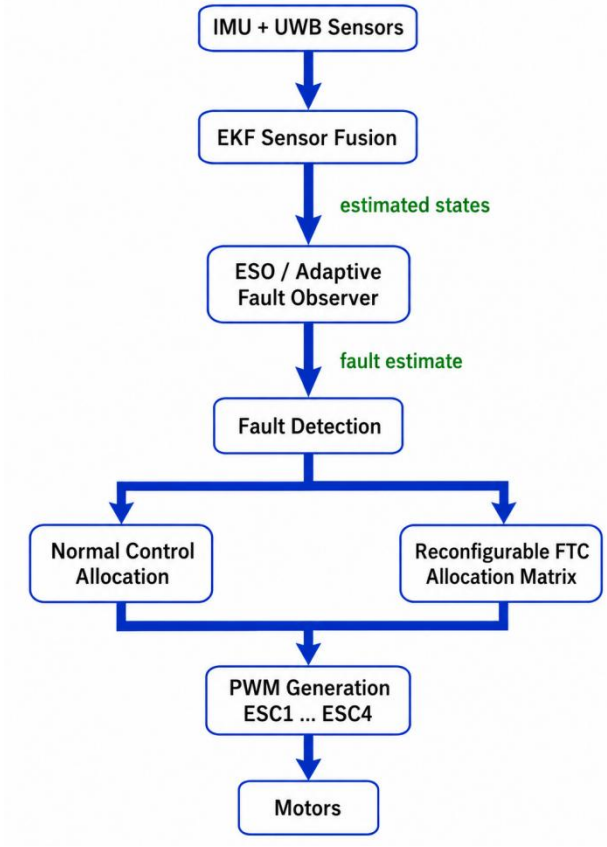

Figure 2: Processing flow per control cycle

The detailed real-time control algorithm with the following execution cycle:

The detailed real-time control algorithm has the following execution cycle: IMU loop ≈ 200 Hz and UWB update ≈ 10–20 Hz. Therefore: FTC loop runs at 200 Hz and UWB correction runs asynchronously when a new packet arrives.

Based on Figure 2, we developed the following algorithm:

WHILE quadcopter active
1. Read IMU
2. Read UWB if available
3. EKF prediction
4. EKF correction
5. ESO state update
6. Estimate disturbances
7. Estimate motor effectiveness
8. Detect fault
9. Reconfigure allocation matrix
10. Compute desired torque
11. Compute new motor thrust
12. Generate PWM
13. Send PWM to ESCs
END

For example, if M4 engine performance declines, the FTC controller will reduce the command for M4, increase Thrust for M3, and adjust M1 and M2 to maintain Roll and Pitch. We use the traditional 3-anchor positioning model described in document [2]. The experimental platform consists of a quadcopter equippedwith an ESP32-WROOM-32 microcontroller, an ICM20602 IMU, a 10-inch frame, and four 9045 CW/CCW propellers. The system integrates a DWM1000 UWB module (tag), a TF-Luna LiDAR, and a 4S 5300 mAh (75C) LiPo battery. The experimental tests were conducted in a workspace with dimensions of 6×6×3 m (L×W×H). Three UWB DWM1000 anchors (Fig. 3) were fixed at three corners of the 6 m×6 m area at a height of 1 m. The coordinates of the anchors are as follows (Fig. 4):

$Anchor_A(0, 0, 1)$, $Anchor_B(6, 0, 1)$, $Anchor_C(0, 6, 1)$

The ICM20602 IMU operates with an internal sampling capability of up to 32 kHz for gyroscope measurements, while the practical controller execution frequency is configured at 200 Hz. The DWM1000 UWB localization system employs a Two-Way Ranging (TWR) mechanism with a practical position update rate of approximately 10–20 Hz, which is sufficient for indoor quadcopter position stabilization and navigation. The TF-Luna LiDAR altitude sensor provides altitude and works in conjunction with 3 UWB anchors to ensure accurate 3D positioning. The ICM-20602 fulfills the project requirements by providing accurate angular data with low latency and seamless integration with the ESP32 via a communication interface. In addition, the combination of IMU and EKF in this case helps eliminate spurious results, smooth the trajectory, and reduce the ambiguity of the results generated by the three UWB anchors.

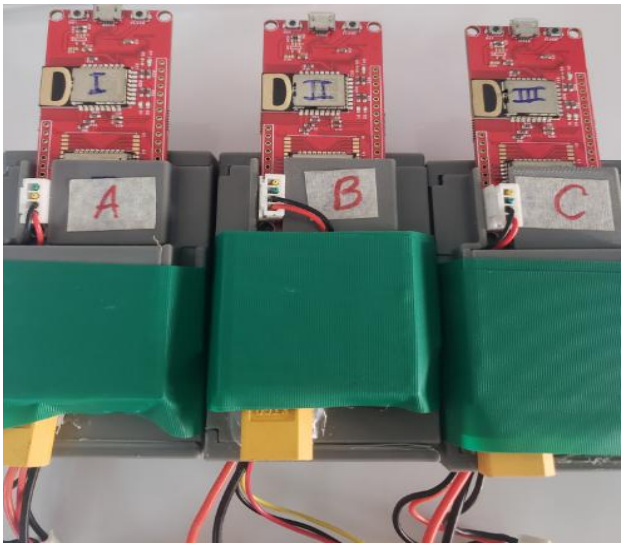

Figure 3: Distribution of Anchors on the testbed.

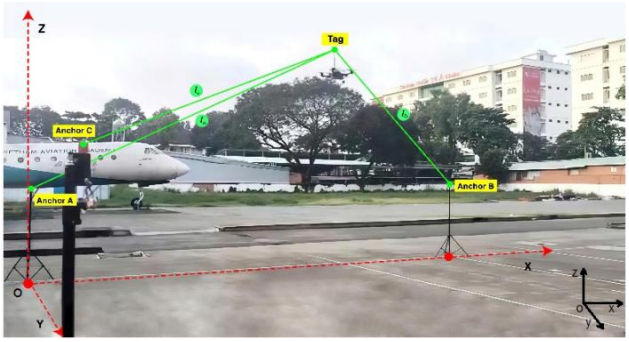

Figure 4: Experimental operation of the quadcopter conducted in a 6×6×3 m (L×W×H) workspace with three UWB anchors fixed at three corners. Note that Anchor C is shown in a close-up view compared to Anchors A and B.

3. Results And Discussion

When motor M4 is weak, the FTC will: reduce the command for M4, increase the thrust for M3, and adjust M1/M2 to maintain roll/pitch. Observations from the experimental phenomenon in Figure 6 and 7 show that PWM_ESC3 increases sharply, while PWM_ESC4 decreases, leading to the appearance of roll oscillation. The results demonstrate that in the event of a single motor experiencing performance degradation, the experimental results demonstrate that the proposed controller maintains stable attitude regulation under actuator fault conditions. Although transient angular-rate oscillations are observed in Fig. 6, the estimated roll and pitch angle tracking errors remain bounded with acceptable RMSE values throughout the experiments. and an average positioning error of less than ±5°, The average position error is less than 0.15 m. When a UWB sensor fault occurs, the proposed adaptive observer enables the system to continue operating stably through IMU–UWB fusion.

Based on Table 3, it is evident that the fault-tolerant controller significantly improves the system's robustness and safety compared to the traditional PID controller

Table 3: Performance comparison between PID and the proposed Fault-Tolerant Control (FTC) system for the quadcopter.

Criterion	PID	FTC
Motor failure	Unstable	Stable
Adaptability	None	Online
Safety	Low	High

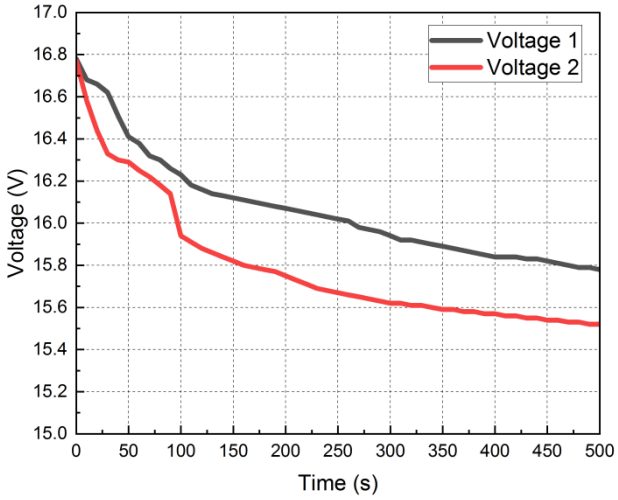

Figure 5: Comparison of LiPo 4S battery voltage levels.

The black curve (Voltage 1) represents the battery voltage under normal operating conditions (all four motors functional), while the red curve (Voltage 2) denotes the voltage during a single-motor failure scenario.

Based on Figure 5, we can see:

Initial Phase (0s to ~50s): Both voltage curves start between 16.7 V and 16.8 V, followed by a rapid decline. This corresponds to the takeoff and initial lift stabilization phase, where all motors accelerate to generate thrust, causing a transient voltage drop due to high current demand. Notably, the Voltage 2 curve exhibits a faster drop compared to Voltage 1; since motor M4 is faulty, motor M3 must increase its thrust to compensate, leading to a higher total current draw and a more significant voltage sag.

Phase 2 (50s to ~150s): The black curve stabilizes, decreasing gradually from 16.4 V to 16.1 V. In contrast, the red curve drops sharply to 15.8 V with an amplitude fluctuation of approximately 0.3 V to 0.5 V. The failure of M4 forces M3 to operate at a higher RPM, consuming more power. Consequently, the flight controller must continuously adjust the roll moment to maintain balance, resulting in persistent small-scale power oscillations.

Phase 3 (150s to ~300s): Voltage 1 remains nearly stable around 16.0 V, whereas Voltage 2 continues to decrease to approximately 15.55 V ($\Delta V \approx 0.4$ V). Due to the motor fault, the quadcopter requires higher power output to maintain altitude, leading to faster battery depletion.

Phase 4 (300s to 500s): Voltage 1 stabilizes around 15.9 V, while Voltage 2 maintains a level of approximately 15.55 V. The system reaches a new steady state where M1 and M2 operate normally, M3 is slightly overloaded, and the thrust of M4 is diminished. The controller maintains level flight by increasing thrust for M3 while simultaneously performing minor pitch/roll adjustments.

In summary, when motor M4 fails, motor M3 compensates for the lost thrust to maintain the UAV's altitude. This compensation increases the power consumption of the propulsion system, leading to a faster battery voltage depletion compared to normal operating conditions. An observed voltage differential of approximately 0.3–0.4 V

indicates higher energy consumption and reduced flight endurance under fault conditions.

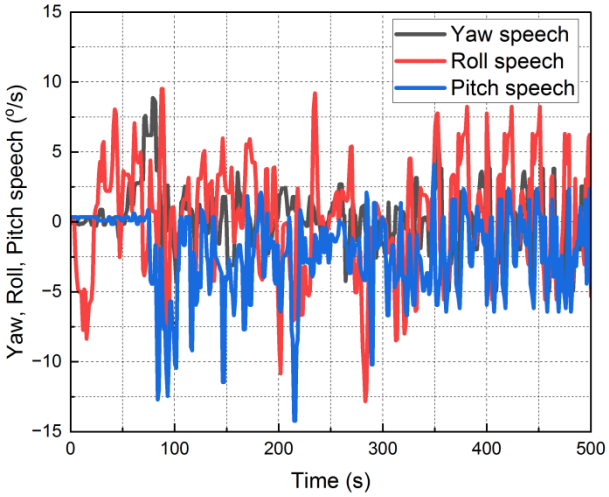

Figure 6: Angular rates of the quadcopter under fault conditions.

Analysis: Observing the graph, it is evident that when motor M4 underperforms, leading to a reduction in lift, motor M3 must increase its speed to compensate and balance the right-side lift of the quadcopter. However, since this compensation is not instantaneously perfect, a continuous small roll moment is generated, forcing the control system to persistently adjust the PWM signals.

Specifically, the Roll Rate (red curve) exhibits oscillations of approximately ±10 deg/s, with larger amplitudes compared to Yaw and the presence of multiple sharp spikes. This indicates that the roll control loop is actively compensating for the unbalanced moment caused by the weakened actuator on one side. Similarly, the Pitch Rate (blue curve) also shows significant fluctuations, ranging from -14 to +5 deg/s. The primary cause is the coupling effect inherent in quadcopter dynamics; as the controller compensates for roll, the varying motor thrusts simultaneously induce small pitch moments. Interestingly, the Yaw Rate (black curve) exhibits significantly smaller oscillations, approximately ±5 deg/s. This phenomenon can be attributed to the fact that yaw control primarily depends on the differential reactive torque between counter-rotating propeller pairs, rather than the thrust degradation of a single motor.

Figure 6 explains the yaw dynamics of a quadcopter as follows: The yaw moment is generated by the difference in reaction torque between the two pairs of wings rotating in opposite directions (Tab 4).

Table 4. Configuring the motors of a quadcopter.

Motor	Rotation direction
M1	CW
M2	CCW
M3	CW
M4	CCW

FTC is compensating with forced redistribution by slightly increasing the speed of motor M2 and slightly decreasing the speed of motor M1 to rebalance reactive torque. In Figure 6, we observe that the Roll oscillation is the largest, the average Pitch and Yaw are the smallest due to the partial degradation of the thrust and the distribution of FTC activity. Roll is more strongly affected than yaw because Motor M4 is offset from the roll axis. At this point, the roll moment is:

$$\tau_\phi = l\left(T_2 + T_3 - T_1 - T_4\right) \quad (23)$$

When thrust M4 decreases, direct lift asymmetry will immediately appear, this is the biggest disturbance.

Meanwhile, with yaw, it only depends on drag torque, but:

Usually: drag torque << thrust force

($k_\tau << k_f$)

therefore, yaw sensitivity is smaller than roll sensitivity.

Furthermore, Figure 6 also shows that Roll/Pitch depends on force imbalance, and Yaw depends on aerodynamic drag imbalance, with aerodynamic drag torque being much smaller than thrust moment. Therefore, we believe that for the same motor attenuation level, roll disturbance is always greater than yaw disturbance.

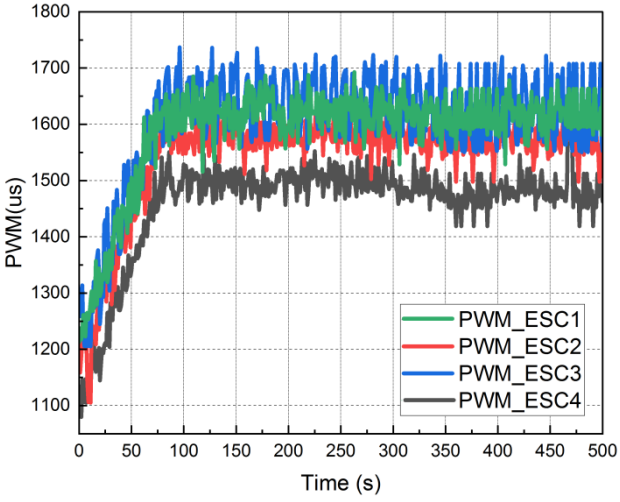

Figure 7: PWM signals for each ESC of the quadcopter under fault conditions.

Consequently, the graph reveals that the Roll Rate contains numerous large spikes, while the Pitch Rate displays strong negative fluctuations. This behavior typically occurs when the control system continuously compensates for thrust imbalances, and the weakened motor introduces a fundamental thrust asymmetry into the system.

The PWM profiles indicate an inherently asymmetrical thrust distribution among the four motors. PWM_ESC4 exhibits the lowest average value, while PWM_ESC3 shows the most significant fluctuations. This behavior suggests that the controller is executing differential thrust adjustments to maintain attitude equilibrium.

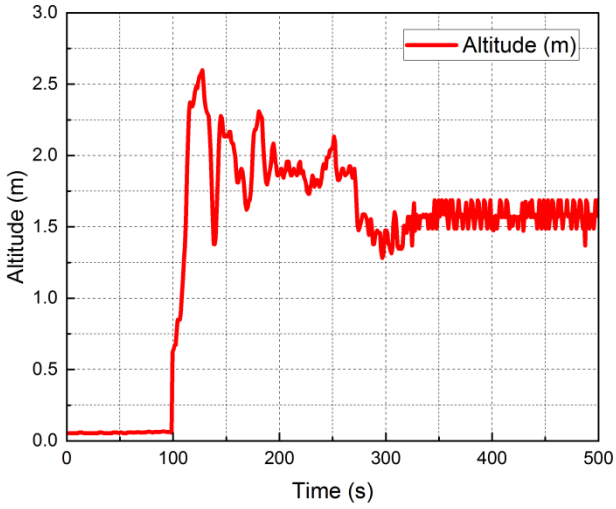

Figure 8: Altitude control experiment with the quadcopter under fault conditions.

Based on the PWM data in Fig. 7, this asymmetry may be attributed to the performance degradation of motor M4, or potentially stem from thrust mismatches between motors, ESC calibration variances, or a shift in the system's Center of Gravity (CoG). The PWM oscillations, ranging from 40 to 80 µs, demonstrate that the PID attitude controller is operating persistently, with motor M3 serving as the primary compensatory actuator in the attitude control loop.

Pre-takeoff Phase (0s – ~100s): The altitude is maintained at approximately z ≈ 5-6 cm as the quadcopter remains on the ground in an idle motor state. The oscillations during this phase are minimal, indicating system stability.

Takeoff Phase (~100s – 140s): The altitude increases rapidly from 0.6 m to 2.6 m. A significant overshoot is observed, which is attributed to the asymmetrical thrust distribution. This imbalance generates a small roll moment, forcing the control system to increase the total thrust to maintain stability, consequently resulting in a larger-than-normal altitude overshoot.

Post-Overshoot Oscillation Phase (~140s – 350s): The altitude fluctuates between 1.8 m and 2.2 m, representing the transient oscillations. Due to the degradation of motor M4, the controller must increase the PWM for motor M3 and continuously adjust the Roll angle. This asymmetrical thrust compensation induces system-wide oscillations, which subsequently result in altitude fluctuations.

Stabilization Phase (~350s – 500s): The altitude decreases to approximately 1.5 m – 1.6 m with reduced oscillation amplitude. This indicates that the controller has successfully reached a new equilibrium point.

The overshoot observed in the graph is relatively high (approximately 40% – 50%) due to the unbalanced thrust. Furthermore, the prolonged oscillations lasting until ~200s demonstrate that the system must persistently compensate for moment imbalances.

In a series of experimental trials, the performance of our Quadcopter controller was evaluated through real-world flight tests. Since the altitude measurement system utilizes an infrared sensor (TF-Luna), the Quadcopter's vertical operating range is restricted to a specific altitude interval to ensure measurement reliability. The experimental scenario was designed following a standard flight cycle consisting of three phases: takeoff, hovering at a predefined altitude, and autonomous landing.

However, in our initial experiments, the reference trajectory for the takeoff phase was constructed as a step signal, which resulted in a significant overshoot in the system response. To improve the transient characteristics or mitigate the effects of a motor failure, the reference trajectory was redesigned as a multi-step input to promptly reduce the gradient of the setpoint signal change. The results shown in Figure 8 demonstrate that this approach enhances the stability of altitude transitions or during a motor failure; nonetheless, the overshoot during the takeoff phase remains relatively large due to the lift compensation provided by motor M3 when motor M4 fails.

In addition to altitude control, the attitude stabilization capability of the Quadcopter was also rigorously evaluated. The results presented in Figure 6 indicate that the controller effectively maintained the Quadcopter's attitude angles. The average errors for the roll and pitch angles reached approximately ~0,83° and ~0,56°, respectively, demonstrating high precision in altitude control during the attitude stabilization process**.**

To further evaluate the reliability of the proposed controller, repeated flight experiments were conducted under identical actuator fault conditions. The tracking performance was quantitatively assessed using Root Mean Square Error (RMSE) and standard deviation metrics.

For the altitude control experiment, the average RMSE was approximately 0.12 m, while the standard deviation remained below 0.08 m during the hovering phase. For attitude stabilization, the roll and pitch angle RMSE values were approximately 1.24° and 0.97°, respectively.

The experimental results demonstrate consistent performance across multiple trials, thereby confirming the repeatability and robustness of the proposed fault-tolerant control framework under motor degradation conditions.

Fig.9 illustrates the overall architecture of the proposed fault-tolerant control framework. The IMU and UWB measurements are fused using an Extended Kalman Filter (EKF) to obtain reliable state estimation. The estimated states are then processed by the adaptive observer to estimate actuator effectiveness degradation. Based on the estimated fault information, the fault-tolerant controller reconfigures the control allocation matrix and generates appropriate motor commands for maintaining stable flight under actuator fault conditions.

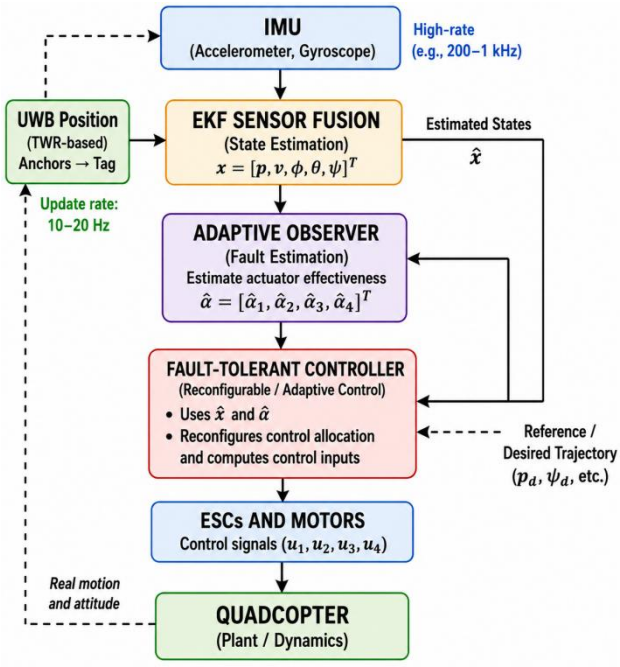

Figure 9: Overall architecture of the proposed IMU–UWB-based fault-tolerant control system for the quadcopter.

4. Conclusion and development direction

This paper has proposed and experimentally validated a UWB-based fault-tolerant control (FTC) framework for quadcopters. The closed-loop system remains locally stable under conditions of partial actuator performance degradation. We can confirm local/conditional asymptotic stability in the case of partial actuator degradation and sufficient remaining control authority. The integration of reconfigurable control, adaptive control, and an observer enables the system to maintain stable flight performance even in the occurrence of motor faults. Future research directions include extending the fault-tolerant methodology to large-scale quadcopters and achieving low-cost autonomous flight capabilities.

Acknowledge

The author thanks Vietnam Aviation Academy for this research.

References

Sebastian Krebs, Tom Herter, Ultra-Wideband (UWB) Positioning System Based on ESP32 and DWM3000 Modules, University of Applied Sciences HTWG Konstanz Alfred-Wachtel-Str. 8, 78462 Konstanz, Germany, 2024.

Zhengrong Xiang et al., An improved UWB indoor positioning approach for UAVs based on the dual-anchor model, Sensor MDPI, 2025.

Loizos Hadjiloizou et al., Onboard real-time multi-sensor pose estimation for indoor quadrotor navigation with intermittent communication, IEEE Globecom Workshops, 2022.

Bouabdallah et al., Design and Control of Quadrotors, IEEE ICRA, 2004.

Blanke et al., Diagnosis and Fault-Tolerant Control, Springer, 2016.

Teixeira et al., Fault-Tolerant Control of UAVs, IEEE Control Systems Magazine, 2010.

Guo et al., UWB-Based Indoor Localization for UAVs, IEEE Sensors Journal, 2019.

Slotine & Li, Applied Nonlinear Control, Prentice Hall, 1991.

P. Pounds, R. Mahony, P. Corke, Modelling and control of a large quadrotor robot, Elsevier, 2010.

Adwait Agawane et al., Autopilot Quad-copter Drone, IJAEM, Vol4, 2022, pp: 1137-1146.